SCIENTIFIC JOURNAL OF MARITIME RESEARCH [POMORSTVO]
University of Rijeka FACULTY OF MARITIME STUDIES

https://doi.org/10.31217/p.40.2.1

CFD Analysis of a Stern Flap Effect on the Hydrodynamics of a Catamaran Ship

Ahmad Firdhaus[1*], Samuel[1], Muhammad Luqman Hakim[1], Ocid Mursid[1,2], Julian Raditya Putra[1]

[1] Department of Naval Architecture, Faculty of Engineering, Diponegoro University, Semarang, Indonesia
[2] Department of Naval Architecture, Ocean and Marine Engineering, University of Strathclyde, Glasgow, UK
[*] Corresponding author: afirdhaus@lecturer.undip.ac.id

ARTICLE INFO

Original scientific paper
Received 1 July 2025
Accepted 21 October 2025

Key words:
Catamaran
Stern Flap
Computational Fluid Dynamic
Ship Resistance

ABSTRACT

Maritime transport is under increasing pressure to improve hydrodynamic efficiency and decrease emissions. Catamarans offer operational benefits; however, they are limited by wave-making resistance at high speeds. Stern flaps are effective for monohulls, but their optimization for catamarans is inadequately investigated owing to the complexities of twin-hull hydrodynamics. This work utilizes computational fluid dynamics simulations to comprehensively assess stern flap performance on a catamaran under varying ship speed conditions and angles of attack. The findings indicate that a 0° flap decreases overall resistance by an average of 5.5%, despite a 1.76% increase in wetted surface area, accomplished by separation-free flow and balanced trim correction, which includes a 42% reduction in stern-squat at higher Froude numbers. Conversely, a 20° flap elevates resistance by up to 8.8% at high Froude numbers due to flow separation, which exacerbates a 4.48% increase in wetted area and a 0.49% rise in heave, despite its 93% geometric trim correction. Research results indicate that neutral flap angles improve catamaran efficiency by avoiding three hydrodynamic drawbacks of higher angles: increased pressure drag, expanded wetted surface, and reduced stability. High-angle configurations are not recommended for any operating profiles.

1 Introduction

Carbon emissions represent a significant worldwide issue, influenced by several variables. Shipping emissions accounted for 2.76% of worldwide anthropogenic emissions in 2012, rising to 2.89% in 2018 [1]. The International Maritime Organization (IMO) has expressed concerns about the environmental implications of shipping, particularly underwater noise pollution, which threatens marine ecosystems and sustainable shipping practices [2,3]. The shipping sector is tasked with developing improvements to enhance ship efficiency. Increased ship efficiency leads to reduced fuel consumption and lower carbon emissions [4]. Enhancing ship design, including hull configuration, propulsion systems, and trim optimization, is a crucial way to reduce fuel consumption and meet sustainability goals by increasing hydrodynamic efficiency through drag reduction [5–8].

Catamarans represent a significant innovation in ship hull design, specifically engineered to enhance hydrodynamic efficiency. Characterized by two parallel hulls connected by a robust deck structure, this multi-hull configuration inherently provides substantial resistance to bending moments and shear forces acting along the vessel's center line [9]. Compared to conventional monohull vessels, catamarans offer distinct advantages, including superior inherent stability and a significantly larger usable deck area [10]. These benefits have driven the widespread adoption of catamaran designs across various maritime sectors, including fast ferries, military vessels, fishing boats, and roll-on/roll-off (ro-ro) ships, establishing them as a prominent solution for specific operational requirements [11]. Although catamarans are more stable and can operate at high speeds, their performance is severely limited by the rapidly increasing wave-making resistance at higher Froude numbers.

Therefore, one of the most critical areas of research in sustainable ship design is the development of efficient resistance-reduction technologies suited to catamaran hull shapes.

Stern flaps are a prominent example of appendage-based innovations developed to improve ship propulsive efficiency. These structures are essentially horizontal extensions fitted to the transom stern [12]. The stern flap's primary function is to modify the flow dynamics around the stern region. By interacting with the hull, stern flaps influence the vessel's trim, reduce propulsion resistance, and can increase operational speed [13]. The underlying mechanism involves reducing the flow velocity beneath the hull, leading to increased local pressure [14]. This elevated pressure generates greater lift and alters the pressure distribution along the stern, resulting in beneficial effects on ship motion and overall resistance [15].

Furthermore, stern flaps enhance the outflow velocity at the trailing edge compared to a baseline hull without a flap. This accelerated flow mitigates adverse flow separation, promotes more favorable separation patterns, and reduces viscous pressure resistance [16]. The performance of a stern flap is critically dependent on three key geometric parameters: chord length, flap angle, and the span across the transom [17]. Theoretical and experimental studies indicate that optimal flap dimensions are speed-dependent; more extended flaps generally offer lower total resistance at lower speeds, while shorter flaps are more effective at higher speeds. Conversely, a larger flap angle tends to reduce drag across a broader speed range [18].

Nevertheless, two significant drawbacks of current parametric research for catamaran applications are its preponderance of monohull configurations, which overlooks twin-hull interference effects and the asymmetric flow fields typical of catamarans, and its lack of investigation into angle-of-attack optimization across the entire speed range. Given the nonlinear resistance properties of catamarans, where wave interference effects peak at particular Froude numbers, this gap is especially significant. Therefore, it is still necessary to systematically quantify the impact of α-influence on catamaran resistance across displacement-to-planning regimes to develop speed-adaptive stern flap solutions.

Although the effectiveness of stern flaps in lowering resistance and increasing propulsive efficiency for monohull vessels has been thoroughly studied, little is known about how to apply them optimally for catamarans. It is not possible to directly extrapolate design principles derived from monohulls due to the fundamentally different hydrodynamics of catamaran sterns, which are characterized by intricate multi-hull interactions, asymmetric flow fields within the central tunnel, and strong wave interference effects at particular Froude numbers [19,20]. Thus, a significant knowledge gap remains: the systematic measurement of stern flap performance, specifically its sensitivity to critical parameters such as angle of attack, for catamaran hulls across the operational speed Froude number range. This gap hinders the development of optimized stern flap configurations that can effectively mitigate the unique resistance characteristics of multi-hull vessels. Addressing this deficit is essential for realizing the full potential of stern flaps as a viable energy-saving technology for the catamaran sector.

The current study employs Computational Fluid Dynamics (CFD) simulations to systematically investigate how the installation of a stern flap affects the resistance characteristics of a catamaran hull, specifically through changes in the stern flap angle (α). To evaluate different stern flap angle configurations over a range of ship speeds representative of typical operating conditions, a parametric CFD study will be conducted. This approach enables a thorough examination of the hydrodynamic elements that affect resistance reduction for every design at various speeds. The primary objectives are to determine the optimal angles for the catamaran design under study and to quantify the impact of changing the stern flap angle on overall resistance. The findings are anticipated to expand the body of knowledge necessary for the successful design and application of stern flap hydrodynamics in multi-hull boats, thereby enhancing the efficiency of catamarans.

2 Materials and Methods

2.1 Geometry Definition and Parameterization

This study references the Delft-372 Catamaran as the ship object of analysis. This ship was selected due to the extensive testing and analysis of the Delft-372 catamaran model by prior researchers [21–23], which will be beneficial in the validation and verification process. Table 1 and Figure 1 present the primary data and visualization of the ship model.

Table 1 Ship main dimension [24].

Dimension	Symbol	Value
Perpendiculars length	Lpp	3.00 m
Beam overall	B	0.94 m
Beam demihull	b	0.24 m
Hull distance	s	0.70 m
Draught	T	0.15 m
Displacement	Δ	87.07 kg
Vertical centre of gravity	KG	0.34 m
Longitudinal centre of gravity	LCG	1.41 m

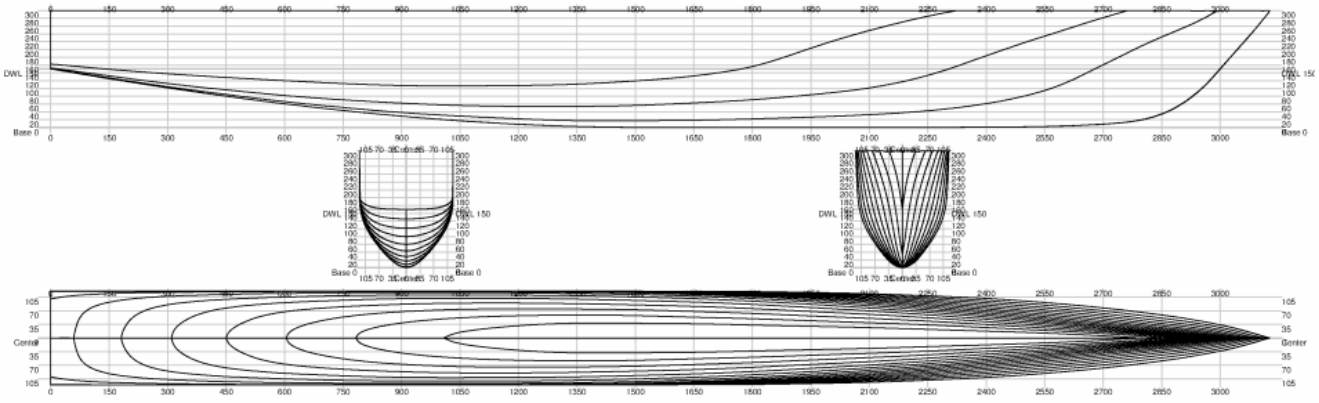

(a)

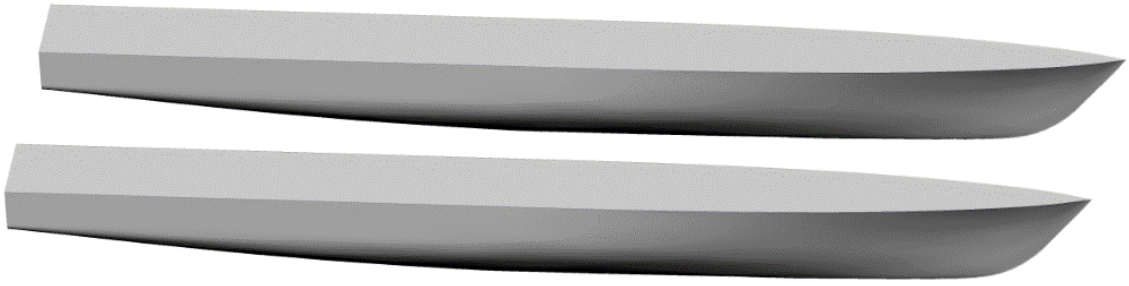

(b)

Figure 1 (a) Linesplan Delft-372 monohull [25], and (b) 3D model of Delft-372 Catamaran.

Research parameters refer to the constraints or methodologies used in the study of measurements. This research employs fixed and variable parameters. The study's fixed parameters are the chord length of the stern flap, whilst the variable parameters consist of the Froude number (*Fr*) and the angle of inclination of the stern flap. Table 2 presents the fixed and variable characteristics of the research. The extent of the stern flap adheres to guidelines from prior research, namely, aligning with the width of the vessel's transom [26]. The simulation technique employs Froude numbers (*Fr*) of 0.3, 0.5, 0.7, 1.0, and 1.3 for each model. Figure 2 illustrates the variance in the configuration of the stern flap.

Table 2 Research parameters.

Variation	Chord length	Angle of attack	Ship speed (*Fr*)
Model 1	2,0% Lpp (0,06 m)	0º	0.3; 0.5; 0.7; 1.0; 1.3
Model 2		10º	
Model 3		20º	

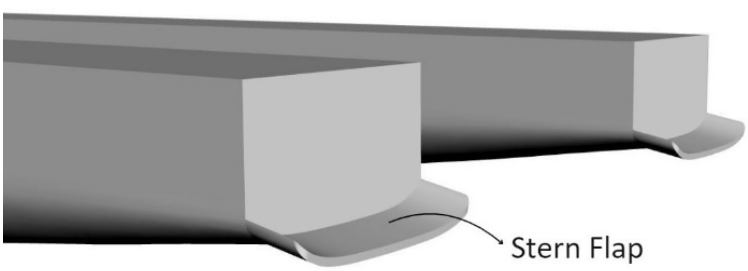

(a)

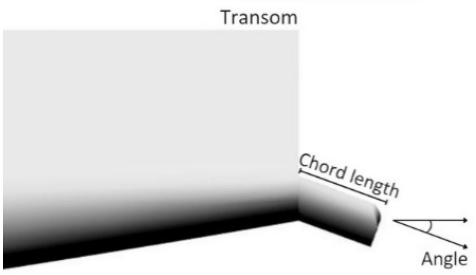

(b)

Figure 2 Stern flap shape: (a) stern flap location, (b) stern flap geometry.

2.2 Numerical Approach

The computational fluid dynamics (CFD) methodology employed in this study is grounded in the fundamental conservation laws governing fluid motion. The continuity equation enforces mass conservation, expressed for incompressible flow as the divergence-free condition of the velocity field, as shown in the equation:

$$\nabla \cdot \mathrm{U} = 0 \tag{1}$$

The vector U represents the speed. The exchange of momentum in a fluid as a function of pressure, viscous forces, and turbulence is defined by the momentum conservation equation, which is provided by the Reynolds-Averaged Navier-Stokes (RANS) equation [27]:

$$\frac{\partial(\rho \mathrm{U})}{\partial t} + \nabla \cdot (\rho \mathrm{UU}) = \\ = -\nabla \mathrm{p} + \nabla \cdot (\mu(\nabla \mathrm{U} + (\nabla \mathrm{U})^T)) + F \tag{2}$$

In this context, p denotes pressure, μ signifies dynamic viscosity, and F indicates external forces. The computational fluid dynamics (CFD) software NUMECA was employed to perform simulations using the k-ω Shear Stress Transport (SST) turbulence model. The transport equation for turbulent kinetic energy (k) delineates the temporal variations of turbulent kinetic energy, governed by production, dissipation, and diffusion. This equation is articulated as follows:

$$\frac{\partial k}{\partial t} + U_j \frac{\partial k}{\partial x_j} = P_k - \beta^* \omega k + \frac{\partial}{\partial x_j}[(v + \sigma_k v_t)\frac{\partial k}{\partial x_j}] \tag{3}$$

The generation of turbulent kinetic energy indicates the conversion of energy from the main flow into turbulence, or P_k. At the same time, $\beta^*\omega k$ represents the rate of turbulent energy dissipation. The second equation, the transport equation for the specific dissipation rate (ϋ), which includes production, dissipation, and diffusion, contains a particular function that permits the transition between the k-ω and k-ε models as follows:

$$\frac{\partial \omega}{\partial t} + U_j \frac{\partial \omega}{\partial x_j} = a\frac{\omega}{k} P_k - \beta\omega^2 + \\ + \frac{\partial}{\partial x_j}\left[(v + \sigma_\omega v_t)\frac{\partial \omega}{\partial x_j}\right] + 2(1 - F_1 \frac{\sigma_{\omega 2}}{\omega}\frac{\partial k}{\partial x_j}\frac{\partial \omega}{\partial x_j}) \tag{4}$$

For the k-ω SST model to handle different flow conditions more successfully, the function F_1. This equation is vital in integrating the features of the k-ω and k-ε models. The k-ω ST model improves flow simulations, especially when it comes to flow events like separation and reattachment [28]. The combination of the k-ω model near surfaces and the k-ε model in the free stream yields more accurate predictions for pressure distribution and skin friction. Thus, employing the k-ω SST model in this study establishes a solid foundation for analyzing complex turbulent flows [29].

The Volume of Fluid (VOF) approach is used to track fluid interfaces in multiphase flow, which involves two or more immiscible fluids, such as water and air. The volume percentage of each computational cell is monitored using the VOF technique, which is controlled by the following equation.

$$\frac{\partial(\alpha_i \rho)}{\partial t} + \nabla \cdot (\alpha_i \rho U) = 0 \tag{5}$$

The volume fraction of phase i is denoted by $\alpha_i\rho$, water density, is denoted by ρ, and the velocity vector is represented by U. In ship hull simulations, this technique is crucial for accurately representing the behavior of phase interfaces, such as the free surface of water.

2.3 Computational Domain and Boundary Conditions

The computational domain and boundary conditions were illustrated in Figure 3, set up following the International Towing Tank Conference (ITTC) Recommended Procedures and Guidelines for Practical CFD Applications [30]. A Cartesian solution domain was created with dimensions based on the catamaran's length between perpendiculars (L). The domain extends 1.5L upstream of the bow to facilitate hydrodynamic inflow development, 4L downstream to account for wake dissipation, 1.5L laterally from the center plane to reduce confinement effects, and vertically from 2L below the baseline to 1.5L pp above the undisturbed free surface. This size meets the basic criteria of ITTC for resistance and propulsion research while enhancing computing efficiency. Geometric symmetry was achieved by setting up a symmetry plane along the vessel's centerline, as per the ITTC.

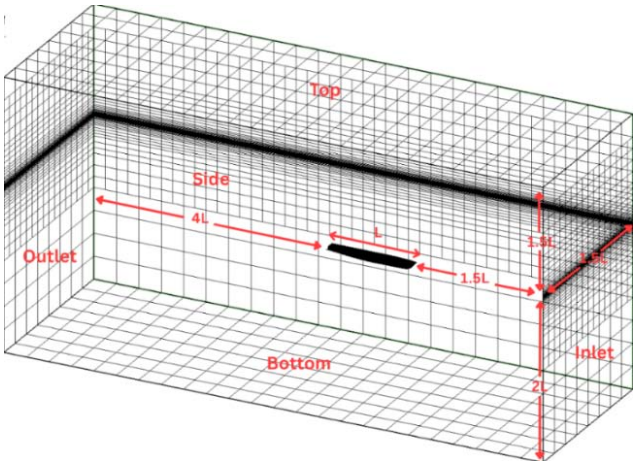

Figure 3 Details of boundary conditions setting and computational domain in conjunction with the simulation model.

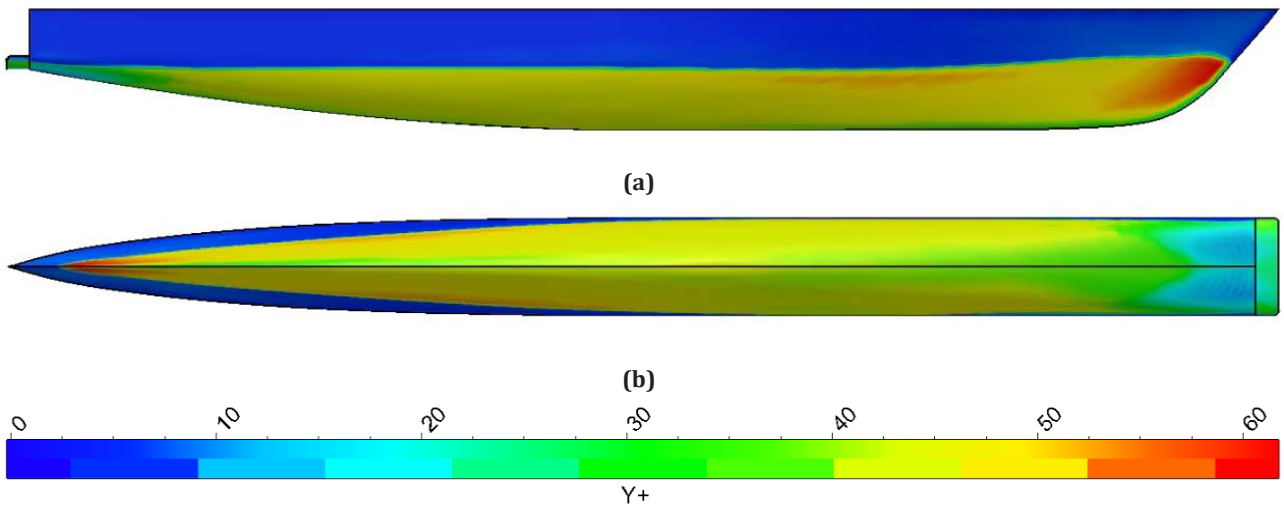

Figure 4 Wall Y+ on catamaran at *Fr* = 0.3 on (a) side view, (b) bottom view

The following were the definitions of the boundary conditions used in this simulation. At the upstream boundary, a velocity inlet is created with a uniform flow of U. To minimize wave reflections, the downstream boundary is equipped with a pressure outlet condition featuring a hydrostatic pressure distribution and wave damping. To simulate unbounded flow conditions, lateral and bottom boundaries were depicted as slip walls. To model the air interface with zero shear stress, the upper boundary was subjected to a symmetry condition. To guarantee resolved viscous boundary layers, no-slip wall conditions were applied to all hull and stern flap surfaces. The Volume of Fluid (VOF) method was used to analyze the air-water interface, with interface sharpening added to minimize numerical diffusion.

The wall distance (Y+) is used in areas where the wall's viscosity has a significant influence on turbulence. The dimensionless distance from the first grid node to the wall surface, Y+, is calculated using the local viscous length scale [31]. According to the 2011 International Towing Tank Conference (ITTC) guidelines, the Y+ value should fall within the range of 30–100 [32]. The calculation can be performed using the formula (6) as follows:

$$Y^{+} = \frac{U_{*}\gamma}{\upsilon} \tag{6}$$

where U_{*} represents the friction velocity at the closest wall, γ denotes the distance to the nearest wall, and υ signifies the local kinematic viscosity of the fluid. Figure 4 presents the Y+ value of the ship, which generally ranges between 40 and 60.

2.4 Mesh Generation Strategy

The quantity of meshes used in CFD research significantly influences the precision of the calculations. An increased number of meshes enhances the accuracy of computational simulations. The mesh refinement technique is advantageous for concentrating mesh density on the vessel's components, particularly on the hull's surface and the ship's curvature, as can be seen in Figure 5. A finer mesh in the concentrated region of the vessel will enable the simulation to more accurately represent flow dynamics and phenomena, including surface waves, turbulence, and complicated viscosity effects [33].

The air-water interface, which is essential for examining wave dynamics, was precisely resolved in this simulation using an adaptive grid refinement technique. Our approach dynamically adjusts the mesh resolution to emphasize directional refinement at the free surface, capturing wave formation and propagation for real-time flow physics simulations. Targeted cell subdivision along wave-aligned orientations and coarsening of non-critical areas were made possible by the refinement process, which identified locations requiring localized grid modifications using flow-derived tensor fields. This technique reduced computing costs by accurately resolving transient wave heights and interface phenomena without refinement zones.

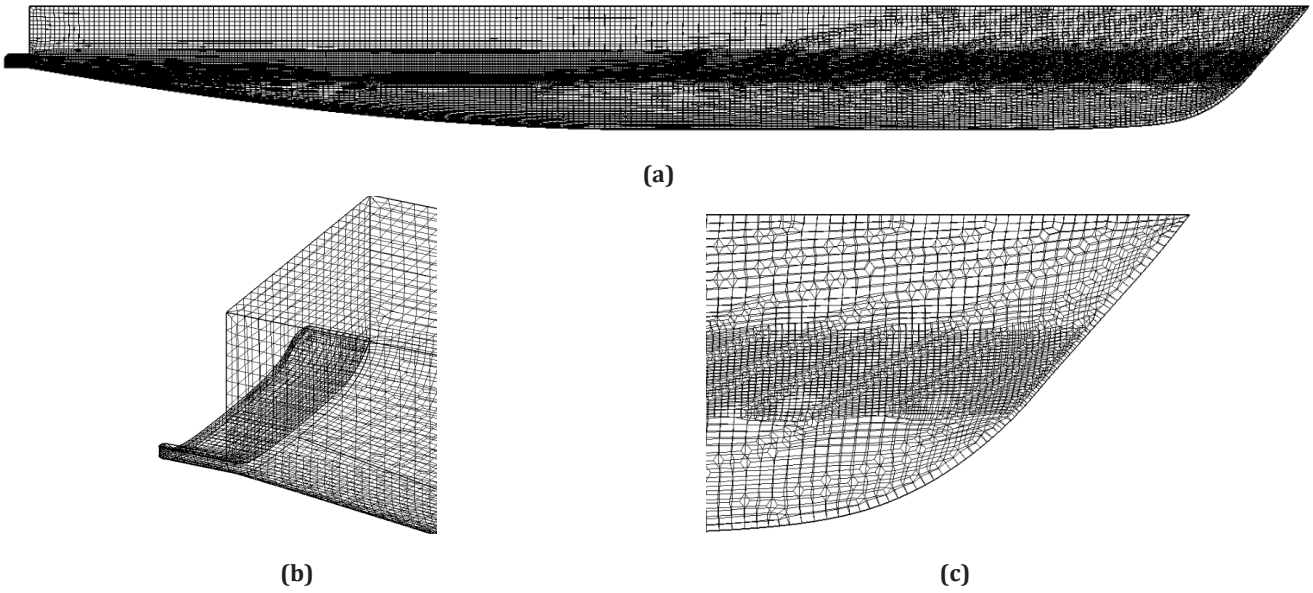

Figure 5 Meshing of the Delft 372 catamaran model, (b) detailed mesh on the stern area, and (c) on the bow area

3 Results and Discussion

3.1 Verification and Validation

The Grid Independence test is conducted to verify the establishment of an optimal balance between total ship resistance and cell quantity, as illustrated in Figure 6. The numerical outcomes were obtained from varying amounts of elements. The mesh was globally refined through successive iterations, uniformly reducing the base cell size throughout the region while maintaining the structured topology. This method ensures that all flow characteristics, such as boundary layers, free-surface waves, and wake areas, are treated uniformly. These are all important for ship simulations. The difference in the number of cells is approximately 1.5 to 2 times greater than the number before [34]. This mismatch is caused by the limitations of the computer processor used in the solver calculation.

Present the results of the grid independence study, showing how the solution converges as the mesh resolution increases. The grid independence analysis indicates that the ideal simulation of the catamaran, conducted with 3.76×10^6. Cells exhibit a total drag force of 13.6 N at Fr = 0.3, accompanied by an optimal

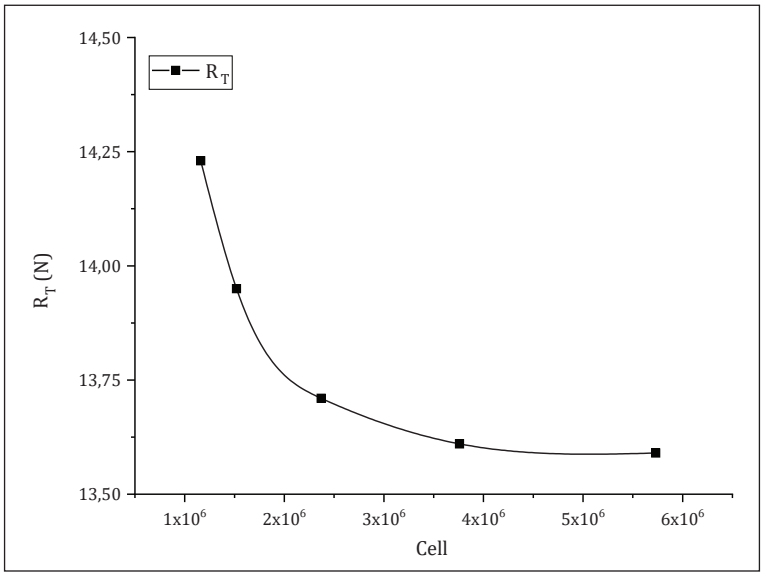

Figure 6 Graph of grid independence illustrating the relationship between cell amount and ship resistance (R_T).

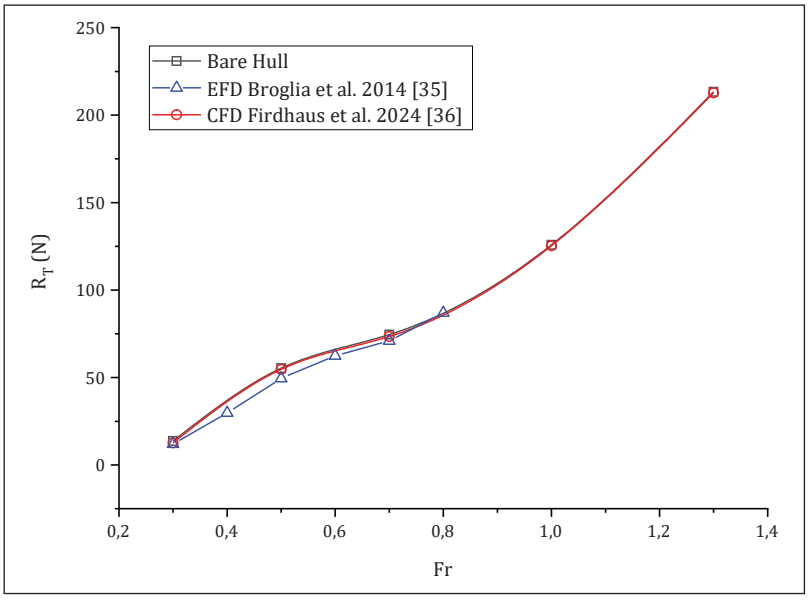

Figure 7 Comparison between the total resistance of the present CFD and the prior experiment [35] and CFD [36] results

resistance variation of 2%. Discuss the point at which further mesh refinement no longer significantly affects the results, justifying the chosen mesh resolution for subsequent simulations.

Through comparing total resistance (R_T) across Froude numbers (*Fr*) with experimental fluid dynamics (EFD) data from Broglia et al. [35] and previous CFD results from Firdhaus et al. [36], Figure 7 validates the current CFD simulation for the bare catamaran hull. The benchmark experiment data and the current CFD results show excellent agreement, especially in the critical *Fr* = 0.35–0.50 range where wave interference effects dominate catamaran resistance. Because transom ventilation modeling in static squat conditions has known limitations, there are slight deviations, less than 4%, at *Fr* = 0.60. However, the overall conformance with the experiment confirms that the free-surface treatment (VOF), turbulence modelling, and mesh resolution strategy have been thoroughly validated for future stern flap simulations.

3.2 Total Resistance

The investigation into the resistance of the flap-induced catamaran was conducted using CFD models by

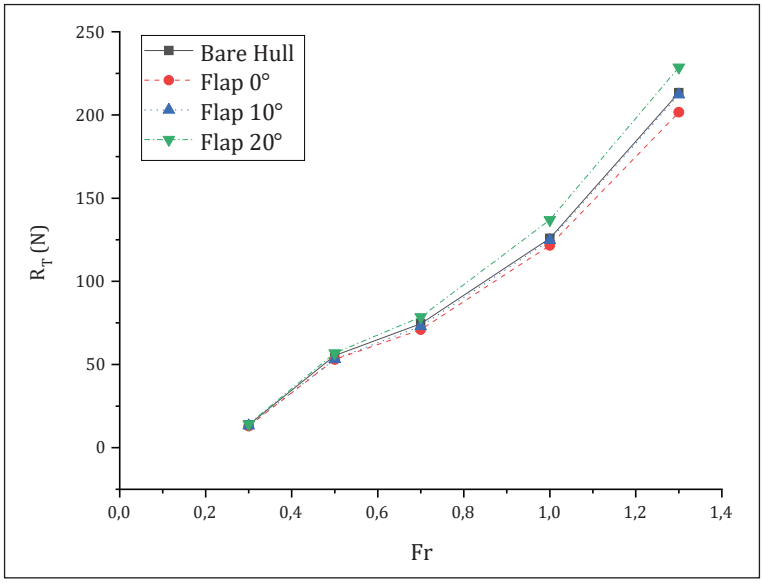

Figure 8 The total resistance of the ship (R_T) for all model configurations as a function of the ship's Froude number.

varying the flap angle of attack and ship Froude number (*Fr*). Figure 8 presents the total resistance (R_T) as a function of *Fr* for the baseline catamaran and three stern flap configurations (α = 0°, 10°, 20°). The data reveal complex angle-dependent and speed-governed interactions that significantly influence hydrodynamic efficiency. The α = 0° configuration consistently reduces resistance across the operational envelope, achieving a reduction of up to 5.5%. This demonstrates that even neutral flap angles yield beneficial flow modification. In contrast, the α = 20° configuration increases resistance at all speeds, with penalties escalating up to 8.8%, indicating detrimental flow separation effects. The performance of the α = 10° configuration exhibits a strong speed dependence: while providing a moderate resistance reduction ofeds, 3.6% at *Fr* = 0.3, its efficacy diminishes sharply at *Fr* > 0.7. Notably, all configurations show limited effectiveness near the wave interference peak, with maximum reduction of only 4.2%, confirming the dominance of twin-hull wave physics over appendage effects in this regime.

The α = 0° configuration delivers the most reliable resistance reduction, establishing it as the baseline recommendation for catamaran applications. While α = 10° maintains marginal benefits below *Fr* = 0.7, its diminishing returns at higher speeds cannot justify implementation over the neutral angle. The severe penalties induced by α = 20° contraindicate its use in any operational profile. These findings necessitate speed-adaptive optimization, where vessels operating predominantly above *Fr* = 0.7 should prioritize α ≤ 0° configurations to avoid performance degradation.

3.3 Wave Characteristic

This subsection addresses the impact of the stern flap on the wave characteristics generated around the catamaran hull. Figure 9 illustrates two top-down views of free-surface wave elevation contours obtained from CFD simulations at a Froude number (*Fr*) of 1. The upper plot represents the bare hull configuration, whereas the lower plot presents the hull equipped with a stern flap at a 0° angle. The wake is characterized by a V-shaped Kelvin pattern in both configurations, modulated by hull interference common to catamaran designs. This pattern consists of transverse and divergent wave components. The observed wakes are narrower than the theoretical deep-water Kelvin wake angle of around 19.47°, aligning with speed-dependent narrowing, where the angle inversely correlates with velocity [37]. The bare hull displays wider, more diffuse wave patterns marked by significant lateral dispersion and increased crest amplitudes (red areas) extending outward, signifying considerable energy dissipation. In contrast, the stern flap variation exhibits more compact, streamlined wave patterns with reduced lateral spread and diminished central interference, indicating improved flow attachment and decreased wave breaking.

A notable distinction in wake angles is illustrated in the bare hull, which presents angles of 17.32°, reflecting a broader V-apex due to unmitigated transom flow separation and rapid stern wave expansion behind the demi hulls. In comparison, the stern flap at 0° results in angles of 16.56°, creating a narrower wake effect that

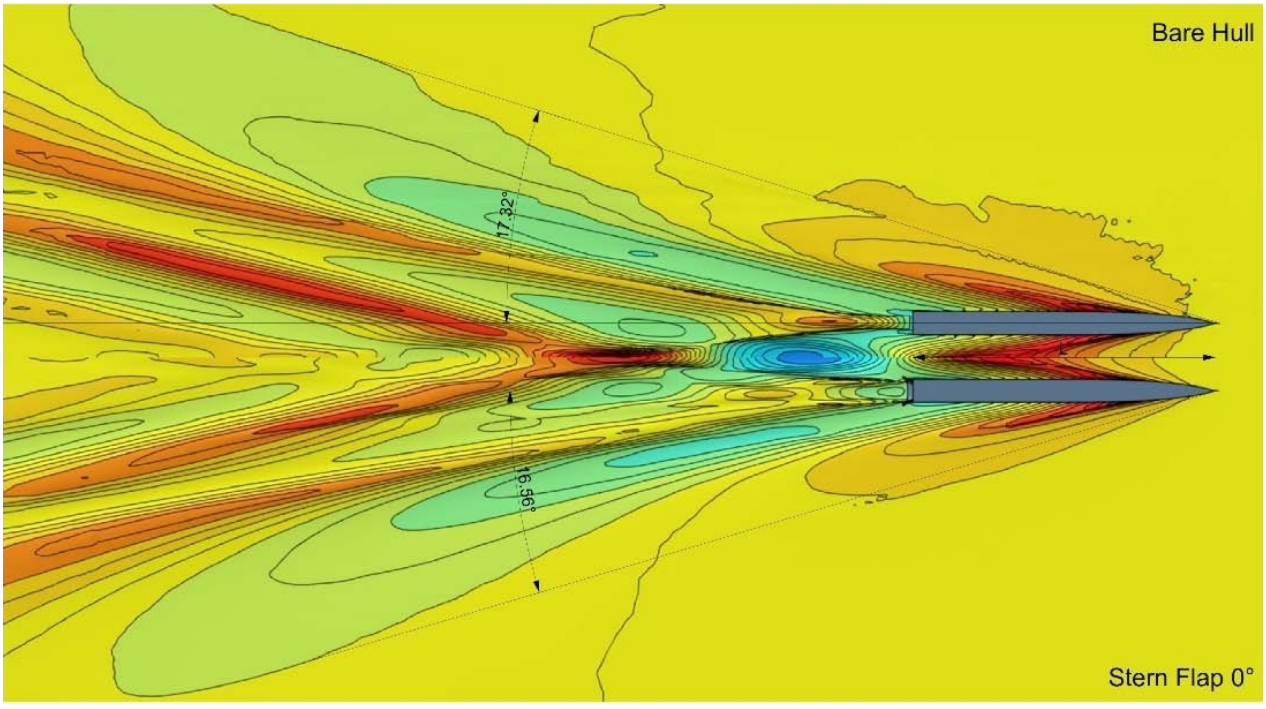

Figure 9 Free-surface contour shows wake angle for bare hull (upper) is wider than stern flap 0° catamaran (lower) at *Fr* 1.

alters stern flow, decreases trim, and reduces divergent wave amplification. The wake angle reduction indicates a reduction in lateral energy radiation in the flapped configuration. Stern flaps optimize hydrodynamic length, suppress interference without increasing frictional drag, enhance seakeeping by mitigating transom losses, and improve efficiency by damping effects. This contrasts with the bare hull, which exhibits a wider wake and increased drag due to heightened wave dispersion. The results demonstrate the effectiveness of stern flaps in improving wake dynamics under neutral deflection, offering essential insights for hydrodynamic optimization in high-speed catamaran design.

3.4 Wetted Surface Area

Figure 10 quantifies the dynamic wetted surface area (WSA) evolution across Froude numbers, revealing a systematic inflation proportional to the stern flap angle, which intensifies with speed, a phenomenon contradicting conventional appendage wisdom. The bare hull exhibits characteristic catamaran behavior; WSA decreases 2.4% from *Fr* =0.3 to 0.5 due to demihull emergence, then increases 21.5% to *Fr* =1.3 from progressive stern immersion. Critically, all stern flap configurations increase WSA relative to baseline, with penalties scaling with angle and velocity. The α=0° configuration maintains the closest alignment to the baseline, while α=10° and α=20° exhibit progressive divergence, reaching maximum WSA expansions of 3.08% and 4.48%, respectively, at *Fr* = 1.3.

These measurements elucidate the trends in ship resistance through hydrodynamic trade-offs. The α=0° configuration's superior resistance reduction, averaging 5.5%, occurs despite minor WSA inflation, as its pressure drag reduction outweighs the frictional penalties. Conversely, α=20° suffers from compounded degradation: its significant WSA expansion amplifies separation-induced pressure drag, resulting in resistance increases of 2.6–8.8%. The transitional behavior of α=10° further demonstrates this mechanism, its moderate 0.17–0.63% WSA inflation at *Fr* ≤0.7 coincides with a measurable reduction in resistance. In comparison, its 3.08% penalty at *Fr* = 1.3 is accompanied by a near-zero benefit in resistance.

3.5 Trim

Figure 11 delineates the dynamic trim characteristics of the catamaran configurations, with negative values indicating stern-down attitude. The results demonstrate that stern flaps systematically reduce stern-down trim across the operational envelope, with efficacy proportional to flap angle yet fundamentally constrained by hydrodynamic separation limits. The bare hull exhibits characteristic squat behavior, progressing from -0.1° at *Fr* = 0.3 to -2.414° at *Fr* = 0.5 before stabilizing near -2.3° at higher speeds. All stern flap configurations counteracted this trend through the generation of hydrodynamic lift, although with markedly divergent efficiency profiles. The α=0° configuration reduced stern-down trim by 32% at *Fr* =0.5 and 42% at *Fr* =1.3, while α=10° achieved 47% reduction at *Fr* =0.5 and 70% at *Fr* =1.3. The α=20° configuration delivered maximum trim correction, with a 58% reduction at *Fr* =0.5 and a 93% reduction at *Fr* =1.3, demonstrating superior geometric potential for attitude control.

These trim modifications resolve the resistance paradoxes identified in total ship resistance. The α=0° configuration's consistent resistance reduction, with an

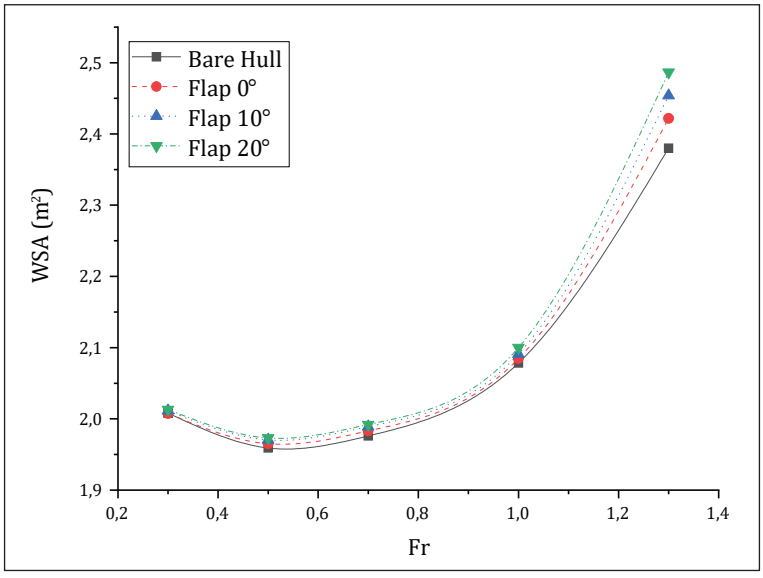

Figure 10 The wetted surface area of the ship (WSA) for all model configurations as a function of the ship's Froude number.

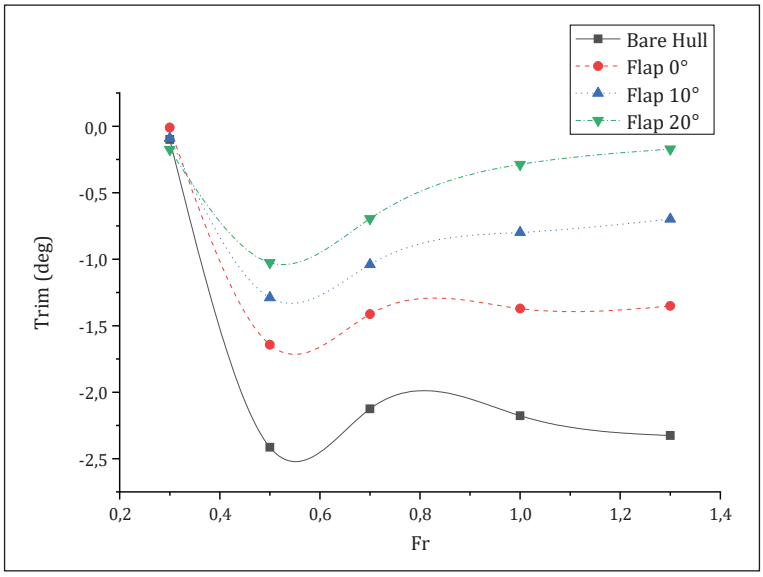

Figure 11 Froude number-dependent ship's trim for all model setups.

average of 5.5%, stems from its ability to maintain flow attachment while providing balanced trim correction. Conversely, α=20°'s aggressive trim correction failed to translate into net performance benefits due to separation-induced degradation. Although achieving a 93% reduction in stern-down trim at *Fr* = 1.3, this configuration simultaneously exhibited an 8.8% increase in resistance at *Fr* = 1.0 and a 4.48% WSA inflation at *Fr* = 1.3. This apparent contradiction is resolved through hydrodynamic trade-offs; the extreme angle provoked boundary layer separation, which amplified pressure drag while diminishing effective lift generation. The transitional behavior of α=10° further validates this mechanism: its initial trim correction advantage at *Fr* =0.5, a 47% reduction, reduced to 70% at *Fr* =1.3, mirroring the decline in resistance reduction from 3.6% to 0.5% across the same speed range.

3.6 Heave

Figure 12 quantifies the heave displacement as a function of speed. At reduced speeds, *Fr* ≤ 0.5, all configurations exhibit nearly uniform heave, which progressively diverges as velocity and flap angle increase. The displacement progression of the baseline hull is notable, reaching a maximum of 0.1888 m (*Fr* = 1.0) and then stabilizing at 0.1837 m (*Fr* = 1.3). The proportional heave elevation induced by stern flaps is most pronounced at elevated speeds: at *Fr* =1.3, α=0° exhibits near-baseline displacement, while α=10° and α=20°

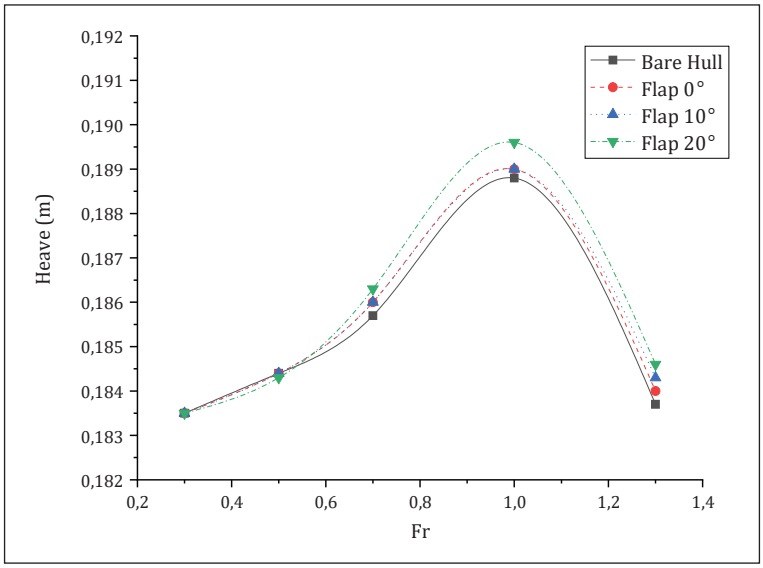

Figure 12 Heave for all model configurations as a function of Froude number.

demonstrate increases of 0.33% and 0.49%, respectively. These patterns provide essential validation of previously identified hydrodynamic interactions. Excessive stern immersion elevates the center of gravity, as demonstrated by a 0.49% increase in heave for α = 20 ° at *Fr* = 1.3 and a 4.48% inflation of the WSA. The maximum resistance penalty at α = 20 ° aligns with the highest heave displacement at *Fr* = 1.0, illustrating the exacerbation of separation-induced drag through the amplification of vertical motion. The progressive increase in heave with flap angle resembles the degradation of trim correction, where flow separation diminishes hydrodynamic lift efficiency despite geometric potential.

Hydrodynamic analysis indicates that heave elevation at elevated angles of attack is due to modified force distribution and heightened energy dissipation. At neutral angles (α = 0°), the arrangement sustains near-baseline heave levels while achieving a 5.5% decrease in resistance. As angles grow, proportionate heave displacement has various detrimental consequences, such as diminished transverse stability owing to a heightened center of gravity, intensified coupled pitch-heave oscillations, and increased resistance penalties from flow separation. Thus, the theoretical lift production at elevated angles, such as α = 20 °, does not improve net efficiency, since the energy required for vertical motion acceleration exceeds any possible advantages.

4 Conclusions

This comprehensive investigation establishes that stern flap optimization for catamarans fundamentally diverges from monohull paradigms, necessitating neutral angles of attack to achieve net efficiency gains. Through rigorously validated RANS-based CFD simulations spanning *Fr* 0.3 to 1.3 and flap angles between 0° and 20°, we demonstrate that zero-degree flap configurations reduce total resistance by an average of 5.5%, despite a minor increase in the wetted surface area, peaking at 1.76%. This performance advantage stems from the balanced generation of hydrodynamic lift, which maintains flow attachment while providing a 32 to 42% reduction in stern-squat, thereby optimizing pressure distribution without provoking separation-induced penalties.

Conversely, higher flap angles exhibit progressively detrimental trade-offs. The 20° stern flap configuration increases resistance by up to 8.8% due to boundary layer separation, which simultaneously amplifies pressure drag, compounds wetted surface expansion to reachng 4.48% at *Fr* 1.3, and elevates heave displacement by 0.49%, despite its superior geometric trim correction of 93%. The 10° configuration exhibits transitional degradation, with resistance reduction declining from 3.6% at a *Fr* of 0.3 to 0.5% at a *Fr* of 1.3 as separation intensifies. These findings resolve a critical industry paradox by revealing that excessive flap angles trigger a hydrodynamic degradation triad, where flow separation consequences negate the theoretical lift benefits.

The universal superiority of 0° stern flap configurations across operational profiles necessitates a paradigm shift in catamaran appendage design. We strongly recommend neutral flap angles for all twin-hull applications, while contraindicating angles of 10° or greater due to significant net efficiency penalties. For vessels requiring enhanced low-speed trim control, integrated solutions should combine neutral flaps with stern wedges rather than adopting higher angles of attack. Future research must prioritize wave-adaptive flap mechanisms for real-world seaways, hybrid configurations with boundary layer control, and full-scale trials incorporating propulsion interactions.

Acknowledgements: This research was funded by the International Publication Research (RPI) fund of the Institute for Research and Community Services (LPPM) at Diponegoro University in 2025, under contract number 222-594.

Author Contributions: Conceptualization, Funding acquisition, Data collection, Methodology, Visualization, Writing original draft, review & editing – Ahmad Firdhaus; Supervision, review & editing – Samuel, Ocid Mursid; Simulation, Review & editing – Muhammad Luqman Hakim, Julian Raditya Putra.

References

[1] International Maritime Organization. *Fourth IMO GHG Study 2020*.; 2021.

[2] Vakili S, Ölçer AI, Ballini F. The development of a transdisciplinary policy framework for shipping companies to mitigate underwater noise pollution from commercial vessels. *Mar Pollut Bull*. 2021;171:112687. doi:10.1016/j.marpolbul.2021.112687

[3] Windén B, Kamiirisa H. Underwater Noise Concerns: How Can the Maritime Industry React? *Journal of Ship Production and Design*. 2024;40(01):1-9. doi:10.5957/JSPD.01220002

[4] Hakim ML, Suastika IK, Utama IKAP. A practical empirical formula for the calculation of ship added friction-resistance due to (bio)fouling. *Ocean Engineering*. 2023;271:113744. doi:10.1016/j.oceaneng.2023.113744

[5] Kiryanto, Hadi ES, Firdhaus A. Total resistance analysis on bow form model ulstein X-bow with various angle of flare and stem angle. *IOP Conf Ser Mater Sci Eng*. 2019;674(1). doi:10.1088/1757-899X/674/1/012003

[6] Samuel S, Yulianti S, Manik P, et al. Numerical Research on the Influence of Interceptor Flaps on the Planing Hydrodynamic Performance. *Naše more*. 2023;70(4):219-227. doi:10.17818/NM/2023/4.4

[7] Firdhaus A, Manik P, Hakim ML, Kiryanto K. CFD Analysis of the Influence of Marine Fouling on the Performance of High-Speed Planning Craft. *Journal of Advanced Research in Fluid Mechanics and Thermal Sciences*. 2023;110(2):124-137. doi:10.37934/arfmts.110.2.124137

[8] Hakim ML, Tuswan T, Firdaus A, Mursid O. INVESTIGATING THE COMPARISON OF SHIP RESISTANCE COMPONENTS BETWEEN U AND V-SHAPED HULLS. *J Teknol*. 2023;85(3):153-164. doi:10.11113/jurnalteknologi.v85.19382

[9] Guo S, Yang X, Li H, et al. Numerical Study on the Influence of Catamaran Hull Arrangement and Demihull Angle on Calm Water Resistance. *J Mar Sci Eng*. 2025;13(4):815. doi:10.3390/jmse13040815

[10] Insel M, Molland AF. An Investigation Into Resistance Components of High Speed Displacement Catamarans. *The RINA*. 1992;134(January):1-20.

[11] Ulgen K, Dhanak MR. Hydrodynamic Performance of a Catamaran in Shallow Waters. *J Mar Sci Eng*. 2022;10(9). doi:10.3390/jmse10091169

[12] Zhou P, Fu J, Zhu J, Xu H. Model Test Study on Parameter Optimization of Stern Flaps of Series Displacement Ships. In: *IOP Conference Series: Earth and Environmental Science*. Vol 219. Institute of Physics Publishing; 2019. doi:10.1088/1755-1315/219/1/012030

[13] Tripathi S, Vijayakumar R. Numerical and experimental study of stern flaps impact on resistance and propulsion of high–speed displacement ships. *Ocean Engineering*. 2024;292:116483. doi:10.1016/j.oceaneng.2023.116483

[14] Song K wei, Guo C yu, Wang C, Sun C, Li P, Wang W. Numerical analysis of the effects of stern flaps on ship resistance and propulsion performance. *Ocean Engineering*. 2019;193:106621. doi:10.1016/j.oceaneng.2019.106621

[15] Jadmiko E, Syarif I, Arif L. *Comparison of Stern Wedge and Stern Flap on Fast Monohull Vessel Resistance*. Vol 3.; 2016.

[16] Budiarto U, Samuel S, Wijaya AA, Yulianti S, Kiryanto K, Iqbal M. Stern Flap Application on Planing Hulls to Improve Resistance. *International Journal of Engineering*. 2022;35(12):2313-2320. doi:10.5829/IJE.2022.35.12C.06

[17] Song K wei, Guo C yu, Wang C, Sun C, Li P, Zhong R fan. Experimental and numerical study on the scale effect of stern flap on ship resistance and flow field. *Ships and Offshore Structures*. 2020;15(9):981-997. doi:10.1080/17445302.2019.1697091

[18] Samuel S, Supriyatin A, Chrismianto D, Zakki AF, Sari DP. Hydrodynamic Analysis of Integrated Interceptor-Stern Flap for Trim Control on High-Speed Planing Vessel. *International Journal of Automotive and Mechanical Engineering*. 2024;21(2):11220-11234. doi:10.15282/ijame.21.2.2024.4.0867

[19] Wulandari AI, Sulisetiyono A, Utama IKAP. CFD Analysis into the Breakdown of Catamaran Resistance Based on the Original Formula by Insel and Molland. *CFD Letters*. 2024;17(5):103-119. doi:10.37934/cfdl.17.5.103119

[20] Samuel S, Iqbal M, Utama IKAP. An Investigation into the Resistance Components of Converting a Traditional Monohull Fishing Vessel into Catamaran Form. *International Journal of Technology*. 2015;6(3):432. doi:10.14716/ijtech.v6i3.940

[21] Farkas A, Degiuli N, Tomljenović I, Martić I. Numerical investigation of interference effects for the Delft 372 catamaran. *Proceedings of the Institution of Mechanical Engineers, Part M: Journal of Engineering for the Maritime Environment*. 2023;238(2):385-394. doi:10.1177/14750902231197886

[22] Broglia R, Zaghi S, Campana EF, et al. Assessment of Computational Fluid Dynamics Capabilities for the Prediction of Three-Dimensional Separated Flows: The DELFT 372 Catamaran in Static Drift Conditions. *J Fluids Eng*. 2019;141(9). doi:10.1115/1.4042752

[23] Firdhaus A, Kiryanto, Zakki AF, Hakim ML, Khalis H. Impact of Surface Roughness on Interference Resistance in Delft 372 Catamarans. *International Journal of Automotive and Mechanical Engineering*. 2025;22(3):12547-12559. doi:10.15282/ijame.22.3.2025.1.0958

[24] Zaghi S, Broglia R, Mascio A Di. Experimental and numerical investigations on fast catamarans interference effects. *Journal of Hydrodynamics*. 2010;22(5 SUPPL. 1):528-533. doi:10.1016/S1001-6058(09)60250-X

[25] Remmlinger U. *The Resistance of the Delft 372 Hull.*; 2014. www.cyberiad.net

[26] Karafiath, Gabor, Dominic S, Cusanelli, Stuart D. Jessup, Christopher D. Barry. Hydrodynamic Efficiency Improvements to the USCG 110 Ft WPB ISLAND Class Patrol Boats. Published online 2001.

[27] Wulandari AI, Utama IKAP, Sulisetyono A, et al. Seakeeping Performance of Warship Catamaran under Varied Hull Separation and Wave Heading Conditions. *Pomorstvo*. 2024;38(2):275-296. doi:10.31217/p.38.2.9

[28] Suastika K, Saputra AS, Fauzi AF, Firdhaus A. Comparison of Performance of Straight- and V-shaped Vanes Applied as Energy Saving Device to High-speed Boats. *CFD Letters*. 2023;15(10):110-122. doi:10.37934/cfdl.15.10.110122

[29] Kiryanto, Budiarto U, Firdhaus A. Analysis of the effect of hull vane on ship resistance using CFD methods. In: *IOP Conference Series: Earth and Environmental Science*. Vol 649. IOP Publishing Ltd; 2021. doi:10.1088/1755-1315/649/1/012051

[30] ITTC. *Recommended Procedures and Guidelines Practical Guidelines for Ship Resistance CFD.*; 2014.

[31] Yonatan Y, Darma E, Hendra Pratama R, Satria IGNA, Dharma Yudha P, Kusuma AI. Impact of Stepped Hull Design on Speed Boat Performance: A CFD Study. *EVERGREEN Joint Journal of Novel Carbon Resource Sciences & Green Asia Strategy*. 2024;11:2580-2589.

[32] ITTC. *Recommended Procedures and Guidelines Practical Guidelines for Ship CFD Applications.*; 2011.

[33] Bilandi RN, Dashtimanesh A, Tavakoli S. Hydrodynamic study of heeled double-stepped planing hulls using CFD and 2D+T method. *Ocean Engineering*. 2020;196. doi:10.1016/j.oceaneng.2019.106813

[34] Anderson JohnD. *Computational Fluid Dynamics; The Basic With Applications.*; 1995.

[35] Broglia R, Jacob B, Zaghi S, Stern F, Olivieri A. Experimental investigation of interference effects for high-speed catamarans. *Ocean Engineering*. 2014;76:75-85. doi:10.1016/j.oceaneng.2013.12.003

[36] Firdhaus A, Kiryanto, Hakim ML, Rindo G, Iqbal M. Ship Performances CFD Analysis of Hydrofoil-Supported High-Speed Catamaran Hull Form. *Journal of Advanced Research in Fluid Mechanics and Thermal Sciences*. 2024;113(1):108-121. doi:10.37934/arfmts.113.1.108121

[37] Darmon A, Benzaquen M, Raphaël E. Kelvin wake pattern at large Froude numbers. *J Fluid Mech*. 2014;738:R3. doi:10.1017/jfm.2013.607